

www.advenergymat.de

# Constructing a Highly Efficient Aligned Conductive Network to Facilitate Depolarized High-Areal-Capacity Electrodes in Li-Ion Batteries

Kai Yang, Luyi Yang, Zijian Wang, Bin Guo, Zhibo Song, Yanda Fu, Yuchen Ji, Mingqiang Liu, Wenguang Zhao, Xinhua Liu,\* Shichun Yang,\* and Feng Pan\*

In order to prepare electrodes with high mass loading and areal capacities, the key issue is to achieve depolarization for both ion and electron transfer on the electrode material surface. In this work, through copolymerization of xanthan gum (XG) and amorphophallus konjac gum (KG) followed by an icetemplating method, aligned electrodes with high areal mass loading of active materials are prepared. In addition to firmly holding active materials together, the prepared KG-XG copolymer also facilitates improved effective porosity as well as homogeneous dispersion of conductive agents (i.e., CNTs). Consequently, with minimum inactive components (i.e., binder and conductive agents), the proposed electrode structure delivers good cycling stability and rate capability under high areal loading (as high as 200 mg cm<sup>-2</sup>). The excellent electrochemical performance can be attributed to the unique aligned structure where the robust conductive network provides an efficient electron and lithium-ion pathway, and the homogenous porosity is beneficial for the electrolyte percolation, hence the reduced polarization during charge transfer. In addition, this electrode preparation method is found to be universal as it is suitable for various types of anode and cathode materials.

1. Introduction

To meet the increasing demand of the high energy/power density electrification equipment and vehicles, high mass loading electrodes with high areal capacity and low inactive component (current collector, conductive carbon, and binder) have attracted numerous attentions. [1] To achieve this goal, electrodes with various structure and component have been reported employing different physical/chemical manufacture process, such as

K. Yang, Dr. L. Yang, Z. Wang, Z. Song, Y. Fu, Y. Ji, M. Liu, W. Zhao, Prof. F. Pan School of Advanced Materials Peking University Shenzhen Graduate School Shenzhen 518055, China

E-mail: panfeng@pkusz.edu.cn B. Guo, Dr. X. Liu, Prof. S. Yang

School of Transportation Science and Engineering

Beihang University Beijing 100191, China

E-mail: liuxinhua19@buaa.edu.cn; yangshichun@buaa.edu.cn

The ORCID identification number(s) for the author(s) of this article can be found under https://doi.org/10.1002/aenm.202100601.

DOI: 10.1002/aenm.202100601

low-temperature sintering,<sup>[2]</sup> freeze casting,<sup>[3]</sup> 3D printing technology, [4] hard template or 3D current collector and molding,[5] graphene and carbon nanotubes (CNTs) skeleton,<sup>[6]</sup> powder extrusion molding (PEM),<sup>[7]</sup> etc. However, with the increasing electrode thickness and areal mass loading, electrochemical performances will be impeded by the sluggish electron/ion transportation. Thick electrodes with aligned structure have been widely explored to create electrodes with low tortuosity and high areal mass loading.[8] It is previously revealed that the effective porosity in the electrode can accelerate ion migration at the electrolyte-electrode interface. [9] Therefore, aligned structures with reduced tortuosity is demonstrated to be beneficial to high areal capacity.[8a] Nevertheless, most aligned electrodes reported are cycled under low current densities which lack of practical and scalable application. Since ion conduction is not an essential issue in

such design, the poor rate capability can be mainly attributed to the poor electronic conductivity across the electrode. Hence, in order to achieve high areal capacity, depolarization for both ion and electron transfer on the electrode material surface should be considered as the priority.<sup>[10]</sup>

In our previous work, CNT network has been proven to depolarize and fully activate the battery performances of NCM materials.<sup>[6d]</sup> However, high areal mass loading cannot be realized without the mechanical support from the robust binder network. In this work, via copolymerization of two nontoxic natural biopolymers (xanthan gum (XG) and amorphophallus konjac gum (KG)) followed by ice-templating method, we demonstrate a new strategy to construct highly efficient electron and lithium-ion conducting pathway in thick electrodes. The KG-XG copolymer forms a robust adhesive network, which facilitates firm fixation of active materials as well as homogeneous dispersion of carbon nanotubes (CNTs) due to the abundant functional groups on KG-XG, which have strong polar interactions with the functional groups on CNTs (Figure 1a). The proposed aligned electrode structure not only enables high areal loading (as high as 200 mg cm<sup>-2</sup>) and low tortuosity, but also allows fast electron conduction utilizing minimum inactive components (i.e., binder and conductive agents). As a result,

16146480, 2021, 22, Dwnholaded from https://dwnneed.onlinelibrary.wiely.com/oi/01002/aena.02200601 by University Town Of Sheraben, Wiley Online Library on [2411025], See he Terms and Conditions (https://onlinelibrary.wiely.com/terms-and-conditions) on Wiley Online Library for rules of use; OA articles are governed by the applicable Cerative Commons

Figure 1. a) Schematic illustration of how KG–XG copolymer interacts with active material and conductive agent, forming an aligned electrode; b,c) microstructures of the aligned structure electrode; d) surface morphology of NCM811 secondary particle fully covered with the CNT conductive network.

greatly improved areal energy and power densities can be achieved. In addition, it is also demonstrated that this method is applicable to a wide range of electrode materials.

#### 2. Results and Discussions

Here we design a robust 3D aligned electrode structure with small amount of biopolymers (1.83 wt%) and CNTs (0.57 wt%). The biopolymer of the XG and amorphophallus KG (the chemical structural formulas are shown in Figures S1 and S2, Supporting Information) are mixed with CNTs and electrode materials, followed by casting and freeze drying. It has been reported that XG exhibits a double helix structure in its aqueous solution owing to the hydrogen bonding interaction between the hydrophobic backbone and the inter/intramolecular branches.[11] Upon the addition of KG solution, the galactose residues on KG molecules will induce copolymerization reactions between XG and KG, forming a much more viscous solution (Figure S3, Supporting Information). Figure S4, Supporting Information, shows the FTIR spectra of the binders, the wide absorption peak centered around 3400 cm<sup>-1</sup> corresponds to the -OH functional groups.[12] The shift in the -OH stretching peak reveals the intermolecular interaction between the copolymers.<sup>[13]</sup> Besides, the abundant -OH groups are reported to provide self-healing ability which will increase the mechanical properties. [12,14] In addition, both the KG-XG solution and the electrode slurry exhibit high viscosity under low concentration (1 wt%) and increased storage modulus, indicating ideal rheology properties (Figure S5, Supporting Information). Consequently, a robust polymer "web" with well aligned structure is constructed, where the active material (i.e., LiNi<sub>0.8</sub>Co<sub>0.1</sub>Mn<sub>0.1</sub>O<sub>2</sub>, NCM811) particles are firmly wrapped (Figure 1b,c). In comparison, the electrode prepared from conventional heat-drying method shows a stacked structure, where the distribution of NCM811 is

dominated by the gravity (Figure S6, Supporting Information). It is noteworthy that despite a low total content (1.83 wt%) of binder, a high areal loading of NCM811 (≈50 mg cm<sup>-2</sup>) can be readily achieved in the aligned structure electrodes. More importantly, being homogeneously dispersed in the binder web owing to the polar interaction, a small amount of CNTs (FTIR spectra is shown in Figure S7, Supporting Information) as electron conductors is able to effectively cover the surface of the active material particles in an CNTs interweaved pattern (Figure 1d and Figure S8, Supporting Information), constructing a highly efficient highway for electron conduction throughout the electrode.

Apart from electronic conductivity, ionic conductivity is equally important in a thick electrode. However, traditional electrodes with stacked structure suffer from low porosity, resulting in low percolation capability for liquid electrolytes. Therefore, concentration polarization will occur at high charge/discharge rates (C-rates), especially for the region deep beneath the electrode surface. The porosity of aligned and stacked electrodes is estimated as shown in Figure S9, Supporting Information, the specific surface and porosity in the aligned electrodes is much larger than the stacked electrodes. To analyze the detailed porosity distribution in the electrodes, scanning electron microscopy (SEM) images (Figure 2a,b) are recognized and analyzed using the Trainable Weka Segmentation (TWS) tool in the ImageJ software. In the overlaid segmentation images (Figure 2c,d), the red, green, and purple regions represent active material, conductive network (binder + CNTs), and pore region, respectively. In the aligned structure electrode, active materials particles are embedded in the cross-linked conductive network to form a directional robust structure with an average void space of 43.0% (detailed component proportion is summarized in Table S1, Supporting Information). By contrast, with a low porosity of 12.5%, the stacked structure electrode also exhibits discontinuous conductive network as well as particle agglomeration. Using the same simulation technique,

16146840, 2021, 22, Downloaded from https://advanced.onlinelibrary.wiley.com/doi/10.1002/nemm.202100601 by University Town Of Shenzhen, Wiley Online Library on [24/11/2025]. See the Terms

and-conditions) on Wiley Online Library for rules of use; OA articles are governed by the applicable Creative Commons

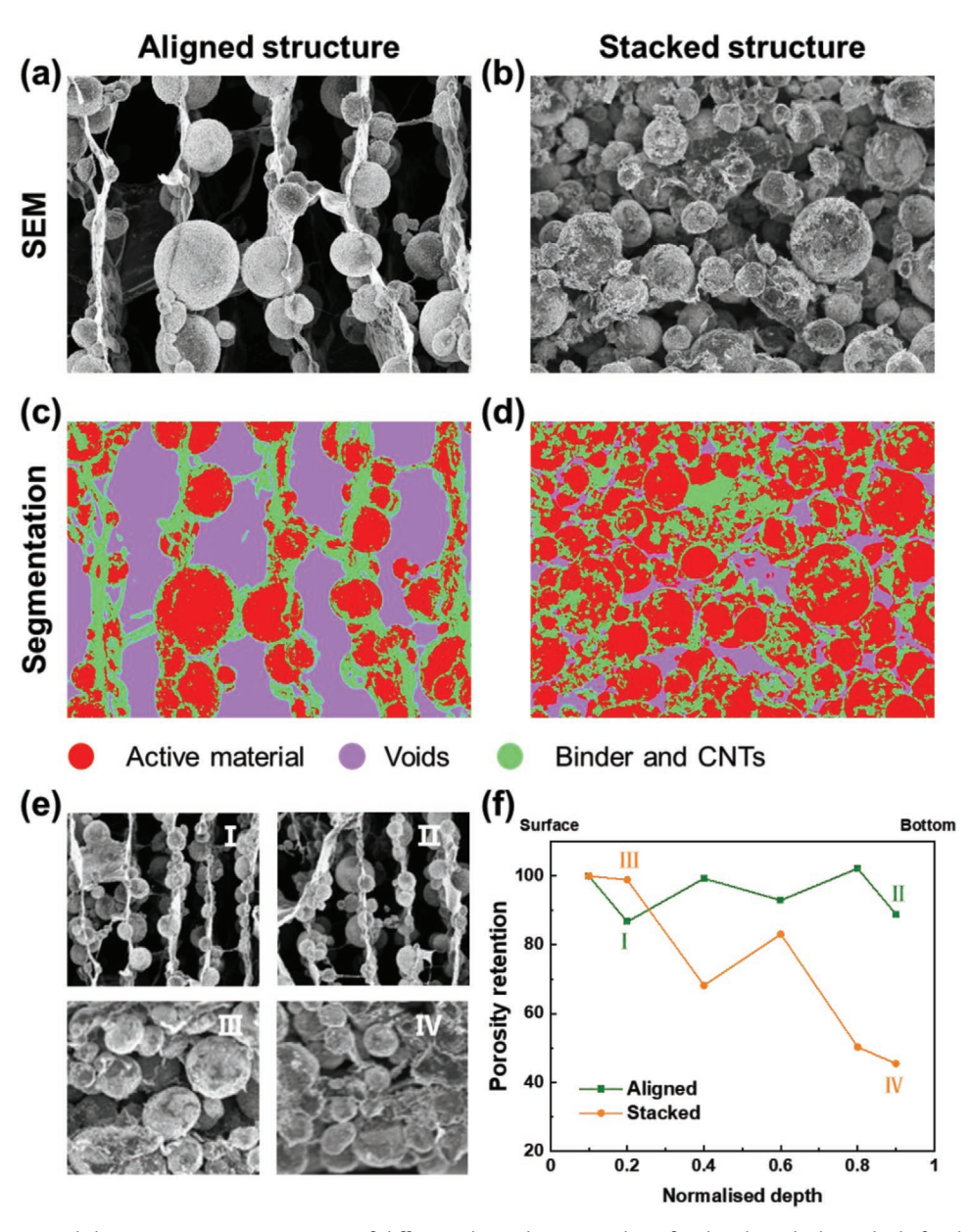


Figure 2. SEM images and the segmentation recognition of different electrodes, (a) and (c) for the aligned, (b) and (d) for the stacked structure electrodes. Typical microstructures and the porosity distribution along the thickness direction, e) SEM images of the four typical regions in different electrodes, and f) porosity retention from the surface to the bottom of the electrodes.

the vertical distributions of voids along the two electrodes are also estimated (Figure 2e). Four different regions (I, II, III, and IV) in the electrodes are selected and compared, it can be observed that the porosity of the aligned structure can be well retained even at the bottom of the electrode, whereas the porosity of stacked electrode gradually decreased from the electrode surface, which is consistent with Figure S6, Supporting Information. This is due to that the conventional heat drying method leads to gradual evaporation of solvent, so the electrode is denser at the bottom. Whereas in the freeze-drying method, the solvent in the slurry is first instantly frozen under a low temperature, then removed by vacuum drying, hence the directional aligned structure can be maintained.

Electrochemical performances of the 3D aligned structure NCM811 electrodes are evaluated through galvanostatic charge/discharge. For the aligned electrode, a specific capacity of 185 mAh g $^{-1}$  (Figure 3a) can be achieved under an areal mass loading of  $\approx\!50$  mg cm $^{-2}$ , which corresponds to an areal capacity of 8.84 mAh cm $^{-2}$ . After 50 cycles, a capacity retention of 92.6% can be achieved (Figure 3b). In comparison, under the same areal loading, the stacked electrode delivers a much lower discharge capacity (average 130 mAh g $^{-1}$  as shown in Figure 3a) and faster capacity decay (Figure 3b). The voltage curves during different cycles are shown in the Figure S10, Supporting Information. Figure 3c compares the rate performances of aligned and stacked electrodes under different current densities. It

www.advancedsciencenews.com

16146840, 2021, 22, Downloaded from https://advancec

onlinelibrary.wiley.com/doi/10.1002/aemm.202100601 by University Town Of Shenzhen, Wiley Online Library on [24/11/2025]. See the Terms

and-conditions) on Wiley Online Library for rules of use; OA articles are governed by the applicable Creative Commons

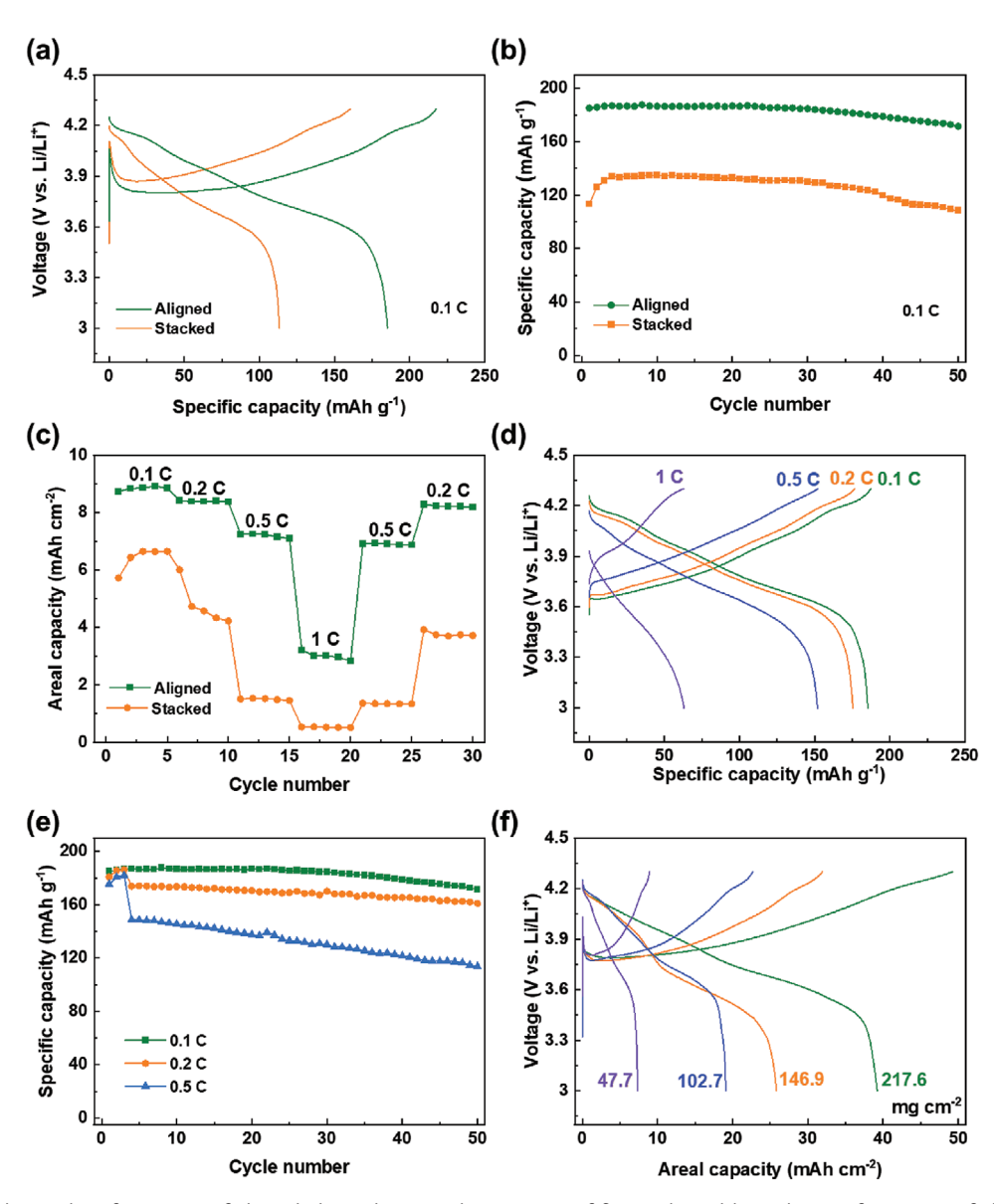


Figure 3. Electrochemical performances of aligned electrodes. a) Voltage curves of first cycle and b) cycling performances of aligned and stacked electrodes under the C-rate of 0.1 C. c) Rate performance of aligned and stacked electrodes. d) Voltage profiles of aligned electrode under different C-rates. e) Cycle performances of aligned electrodes at different C-rates. All areal mass loading of NCM811 above is  $\approx$ 50 mg cm<sup>-2</sup>. f) Voltage curves of the aligned structure electrodes under different areal mass loading of NCM811 at 0.1 C.

can be seen that the aligned structure shows not only a higher initial capacity, but also a much improved rate capability owing to the fast charge transfer process within the electrode. Figure S11, Supporting Information, shows the EIS comparison of the different electrodes before cycling. The aligned structure electrode shows the smallest charge transfer resistance (indicated by the semicircle). Lithium ion diffusion coefficient  $^{[15]}$  in the aligned structure electrode is calculated to be 1.244  $\times$   $10^{-9}$  S cm $^{-2}$  as shown in the Figures S12 and S13, Supporting Information, which is comparative to the low mass loading electrodes in the literatures.  $^{[15a]}$  There have been plenty of literatures reporting high areal mass loading electrodes, unfortunately many of them can only be operated under extremely low C-rates (usually no more than 0.01 C), which is impractical for

general uses. The sudden capacity drop from 0.5 to 1 C is very likely to be limited by the Li-ion diffusion across the relatively thick electrode. In the future, this intrinsic issue could be tuned through optimizing electrode structure and electrolyte composition. From the voltage profiles (Figure 3d), it can be observed that the overpotentials of aligned electrode is relatively low under practical C-rates. The excellent electrochemical performances can be attributed to the robust conductive network can provide sufficient electron pathway and the aligned structure is beneficial for the electrolyte percolation, which will greatly decrease the polarization and improve the depth of discharge. Moreover, the 3D aligned structure electrode can be stably cycled under higher C-rates of 0.2 and 0.5 C, achieving capacity retention of 92.5% and 76.3% after 50 cycles, respectively. (Figure 3e, and the voltage

16146840, 2021, 22. Downloaded from https://advanced.onlinelibrary.viley.com/ob/10.1002/aemm. 202100601 by University Town Of Shenzhen, Wiley Online Library on [24112025]. See the Terms and Conditions (https://onlinelibrary.wiley

and-conditions) on Wiley Online Library for rules of use; OA articles are governed by the applicable Creative Commons

profiles are shown in Figure S14, Supporting Information, long cycle performances are shown in the Figures S15 and S16, Supporting Information). The aligned structure can maintain during the electrochemical cycling as shown in the Figure S17, Supporting Information, which confirms the mechanical stability of the demonstrating electrodes.

As the copolymer interactions of biopolymers can create a robust binder network with mechanical stability, attempts have been made to further increase the areal mass loading. Increasing amounts of NCM811 particles have been added during the slurry preparation process. Figures S18a to S18c, Supporting Information, show the SEM images of electrodes with areal mass loadings of 102.7, 146.9, and 217.6 mg cm<sup>-2</sup>, respectively. With the increasing areal mass loading, the aligned structures can be retained in spite of the decreasing porosity. As expected, higher initial areal capacities of 19.1, 25.8, and 39.3 mAh cm<sup>-2</sup> for the three electrodes shown above (Figure 3f), which correspond to specific capacities of 186, 181, and 177 mAh g-1 (Figures S18d to S18f, Supporting Information), respectively. This result suggests that in principle, the electron conductive network and the aligned structure within the electrodes could still work properly at such high loading and minimum inactive components (the component proportion is summarized in Table S2, Supporting Information). As contrast, the high areal mass loading PVDF based electrodes are also prepared as shown in Figure S19, Supporting Information, cracks are found on the electrode surface owing to the

insufficient mechanical support, while the height of the aligned structure electrode can be elevated to several millimeters remaining in structure integrality (shown in Figure S20, Supporting Information). Freeze drying method is also employed to PVDF-based electrodes (Figure S21, Supporting Information). Unfortunately, after freeze-drying, the electrode crimped, and cracks were created as shown in Figure S21b, Supporting Information. Different parallel experiments show the same results. It can be speculated that PVDF cannot provide enough mechanical support during the electrode preparation, which instead shows the robust mechanical stability of the demonstrated biopolymers and aligned electrodes in our work. After 20 cycles, the aligned electrodes with areal loading of 102.74 and 146.9 mg cm<sup>-2</sup> can still deliver capacity retention of 83.7% and 77.0%, respectively. However, when the mass loading is 217.6 mg cm<sup>-2</sup>, the capacity quickly fades with cycle numbers, which is possibly owing to the accelerated consumption of the electrolyte from side reactions.

To test the versatility of the proposed electrode structure, active materials with different operating voltages including Li<sub>1.2</sub>Mn<sub>0.54</sub>Ni<sub>0.13</sub>Co<sub>0.13</sub>O<sub>2</sub> (Li-rich), graphite and SiO<sub>x</sub>@C (corresponding XRD patterns are shown in Figure S22, Supporting Information) are selected. From the SEM images (Figure 4a and Figure S23, Supporting Information), it can be seen that although the morphology of different electrodes varies owing to the different particle sizes and morphologies, the aligned structures can still be observed clearly. For all active materials, as the

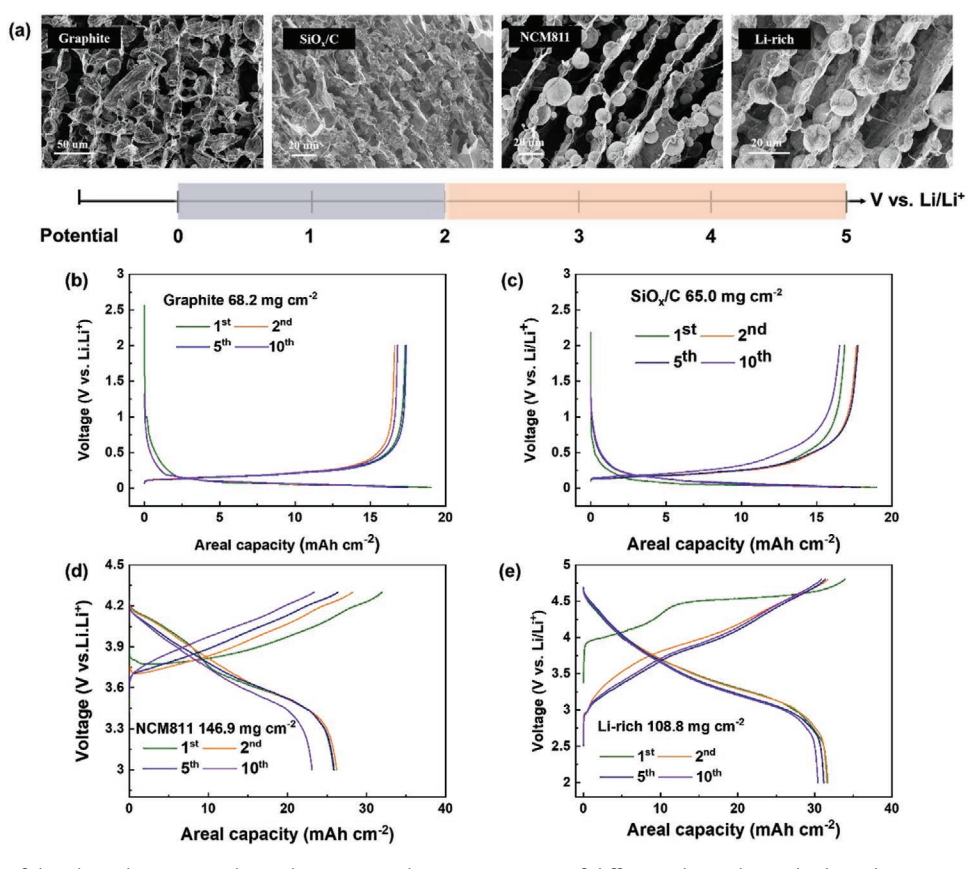


Figure 4. Versatility of the aligned structure electrodes. a) Typical microstructures of different electrodes with aligned structures including graphite, SiO<sub>x</sub>/C, NCM811, and Li-rich. b-e) Voltage curves and the areal capacity of the different electrodes at 0.1 C.

www.advancedsciencenews.com

www.advenergymat.de

16146840, 2021, 22, Downloaded from https://advanced.onlinelibrary.wiley.com/doi/10.1002/aemn.202100601 by University Town Of Shenzhen, Wiley Online Library on [24/11/2025]. See the Terms and Conditions (https://onlinelibrary.wiley.com/terms-

and-conditions) on Wiley Online Library for rules of use; OA articles are governed by the applicable Creative Commons

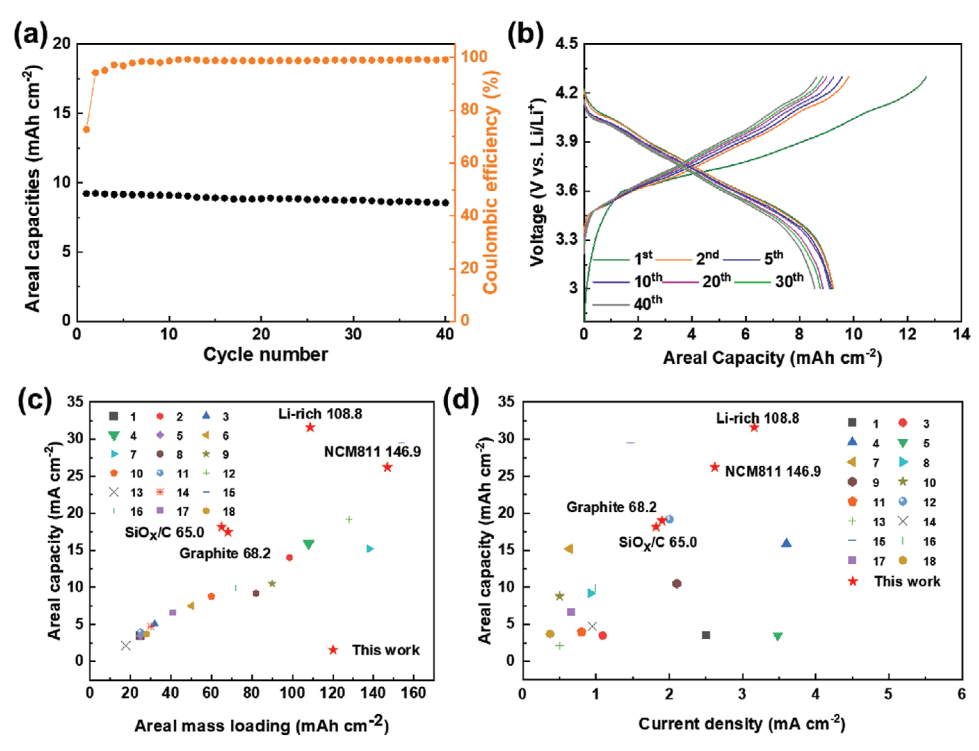


Figure 5. Comparison of the electrochemical performances with literatures. a) Cycling performances of full battery with aligned cathode (NCM811) and anode (graphite) at 0.1 C. b) Voltage curves in different cycles of the full battery. c) The areal mass loading and capacity comparison with literatures. d) The comparison of areal capacity versus current density with published results. Detailed information and the references are listed in Table S3, Supporting Information.

areal mass loading increases, the porosity decreases while the aligned structures remain (Figure S24, Supporting Information).

Under a wide range of an electrochemical window from 0 to 4.6 V (versus Li/Li<sup>+</sup>), all electrodes show good cycle stability as shown in Figure 4b–e. Considering that graphite and the SiO<sub>x</sub>/C electrodes will undergo volume change during electrochemical cycling, the areal mass loading of these electrodes is controlled between 60-70 mg cm<sup>-2</sup>, which is still four times higher than the commercial electrodes. The resulting areal capacity can be elevated to 17.3 and 16.9 mAh cm<sup>-2</sup> for graphite and SiO<sub>x</sub>/C electrodes, respectively. As for the cathode electrodes, all the areal mass loading can be elevated to more than 100 mg cm<sup>-2</sup>. Under the current density of 0.1 C, the areal capacity can be elevated to 33.9 mAh cm<sup>-2</sup> for the Li-rich (108.8 mg cm<sup>-2</sup>) electrodes. The Coulombic efficiency (CE) of the various electrodes during cycles is shown in the Figures S25 and S26, Supporting Information. Table S3, Supporting Information, summarizes the first CE and average CE during cycles of various electrodes. The average coulombic efficiency of the aligned structure electrodes is more than 99% which is at the same level of the low mass loading PVDFbased electrodes. The practical cycling of the electrodes with high CE confirms the electrochemical stability of the biopolymers.

The versatility of aligned structure in both cathode and anode electrodes allows us to fabricate high areal capacity full cells. While many similar electrode designs can be only cycled under impractically low C-rates (1/30 C, 1/25 C, etc.), we aim to cycle the full cell under 0.1 C to make it more practical. In the full cell, aligned NCM811 electrode (about 45–55 mg cm<sup>-2</sup>) are selected as the cathode and aligned graphite electrode with

matching areal capacity ( $\approx$ 20% excess) is selected as the anode. As shown in **Figure 5**a, the NCM811/graphite full battery can deliver an areal capacity of 9.2 mAh cm<sup>-2</sup> under 0.1 C and a high capacity retention of 92.8% after 40 cycles (the voltage curves are shown in Figure 5b).

The Ragone plot for the thick electrodes with various areal mass loading compared with the state-of-the-art electrodes in half-cells and full cells is shown in Figure 5c,d. The copolymer interactions of the biopolymers help to build a robust network to support the high areal mass loading. The CNTs are homogeneously dispersed in the network of binders and the surface of the electrode particles, which can ensure the sufficient electron transformation. The ice-plating and vacuum cold drying technique helps to create the aligned electrode structure to boost the ionic exchange on the electrode surface. Comparatively, while many thick electrodes can be only cycled under a low current density (such as 0.01 C, 0.04 C, etc.), all the electrodes in our work are cycled under the current density of 0.1 C (Figure 5d). With the demonstrated biopolymers and the electrode preparing technique, the areal mass loading can be elevated up to 217.7 mg cm<sup>-2</sup> for the thick NCM811 electrodes (Figure 5c and Table S4, Supporting Information). And the thick LMO electrodes can deliver a high areal capacity of 31.6 mAh cm<sup>-2</sup>.

### 3. Conclusion

To sum up, through copolymerization of XG and KG followed by ice-templating method, highly efficient electron/ion



www.advancedsciencenews.com

www.advenergymat.de

ADVANCED ENERGY MATERIALS

conducting pathways are built in an aligned electrode with high areal mass loading of active materials while a minimum inactive component (binder and conductive agents) is required. As the adhesive network, KG-XG copolymer provides not only a firm binding force for active materials, but also polar interaction with conductive agents (i.e., CNTs), which allows homogeneous dispersion of CNTs. Consequently, with minimum inactive components, the proposed electrode structure delivers good cycling stability and rate capability under high areal loading (as high as 200 mg cm<sup>-2</sup>). The excellent electrochemical performances can be attributed to the robust conductive network can provide sufficient electron pathway and the aligned structure is beneficial for the electrolyte percolation, which will greatly decrease the polarization and improve the depth of discharge. Therefore, this universal electrode preparation method opens up a new strategy to achieve practical electrodes with high areal capacities.

## 4. Experimental Section

Synthesis of the Thick Electrode: Xanthan gum (XG, Aladdin, China) and konjac glucomannan (KG, China) were first dissolved in deionized water separately at a mass ratio of 1 wt% and oil bath heated at 70 °C for 8 h. The resulting XG and KG solution were mixed with CNT aqueous dispersion (0.4 wt% SWCNT in water, ≈0.2 wt% carboxymethyl cellulose as a surfactant stabilizer, Tuball, OCSiAl) in a volume ratio of 1:1 separately and labelled as XG@CNT and KG@CNT solution. Different electrode materials were chosen to synthesize thick electrodes. For example, 2 grams of NCM811 (LiNi<sub>0.8</sub>Mn<sub>0.1</sub>Co<sub>0.1</sub>O<sub>2</sub>, Ningbo Jinhelidian) were added into 2.5 mL of XG@CNT solution and 5 ml of KG@CNT solution; the mixture was grinded in the mortar to get well-dispersed electrode slurry. The resulting slurry was casted onto copper plate and froze with liquid nitrogen. The obtained sample was quickly transferred to the freeze dryer for 24 h. The electrode with different mass loading was fabricated by controlling the NCM811 mass (2, 4, 6, and 8 g). Other thick electrodes were prepared following the same procedure, such as Li-rich (Li<sub>1.2</sub>Mn<sub>0.54</sub>Ni<sub>0.13</sub>Co<sub>0.13</sub>O<sub>2</sub>, Ningbo Fuli Battery Materials Technology Co., Ltd), SiO<sub>x</sub>/C (BTR), graphite (Shenzhen MTI). Traditional PVDF (poly(vinylidene fluoride)) electrode was prepared by casting the NCM811 slurry on the aluminum foil and drying in the vacuum oven at 80 °C overnight. The slurry was prepared by mixing 80 wt% NCM811 particles, 10 wt% acetylene black (AB), and 10 wt% PVDF dissolved in N-methyl-pyrrolidone (NMP).

Materials Characterizations: The rheological properties of the slurry were measured by rheometer (HAAKE, USA). FTIR spectra were measured on a Nicolet Avatar 360 spectrophotometer (KBr tablet). The porosity of thick electrode was measured on a Mercury porosimeter (AutoPore IV 9500). The microstructures and chemical component of the thick electrode were characterized by SEM (Zeiss SUPRA55) and energy dispersive spectrometer (EDS). The X-Ray Diffraction (XRD) was performed on the Bruker D8 Advance powder X-ray diffractometer with  $2\theta$  in the range of 10– $90^{\circ}$  with a count time of 0.1 s per step.

Electrochemical Testing: The electrochemical performance of the traditional electrodes was tested using 2032-type coin cells with electrode diameter of 10 mm. The electrochemical performance of thick electrodes was investigated using a cartridge cell with diameter of 1/2 inch. All the batteries and cells were assembled in an Argon-filled glovebox with  $\rm H_2O$  and  $\rm O_2$  contents below 0.1 ppm. Lithium foil was used as reference/counter electrode. The electrolyte was 1 M Lithium hexafluorophosphate (LiPF6) in ethylene carbonate/ethyl methyl carbonate (EC/EMC, 3:7 in volume ratio, DoDochem). Galvanostatic charge—discharge cycling tests were carried out by Neware Testing system (Shenzhen NEWARE Electronics Co., Ltd.). Electrochemical impedance measurements (EIS) were tested using a Solartron 1470E electrochemical workstation with

a frequency range of 1 MHz to 0.1 Hz. The areal capacities (C/A) of the electrodes were obtained by dividing the measured cell capacity by the geometric electrode area. The full cells were assembled by pairing graphite anodes with NCM811 cathodes. The N/P ratio is the capacity ratio between the anode and cathode, was fixed to be 1.2/1. GITT was carried out under the current density of 0.1 C. Before GITT test, the battery had been cycled for 2 cycles. The pulse time and relaxation time were 15 and 30 min, respectively.

### **Supporting Information**

Supporting Information is available from the Wiley Online Library or from the author.

## Acknowledgements

K.Y., L.Y., Z.W. contributed equally to this work. This research was financially supported by National Key R&D Program of China (2016YFB0100300), National Key R&D Program of China (2016YFB0700600), the Shenzhen Science and Technology Research Grant (JCYJ20200109140416788), the Chemistry and Chemical Engineering Guangdong Laboratory (Grant No.19220180), National Key R&D Program of China (2020YFB07045000).

#### **Conflict of Interest**

The authors declare no conflict of interest.

## **Data Availability Statement**

Research data are not shared.

## Keywords

aligned structures, binder design, conductive networks, high areal capacity, thick electrodes

Received: February 20, 2021 Revised: March 31, 2021 Published online: April 24, 2021 1614849, 2021, 22 Dwnholoded from https://atvanced.onlinelibrary.wiely.com/oi/010.002/aem.20.2010.0601 by University Town Of Shezhem, Wiley Online Library on [2411.0225]. See the Terms and Conditions (https://onlinelibrary.wiely.com/terms-and-conditions) on Wiley Online Library for rules of use; OA articles are governed by the applicable Cerative Commons

- [1] Y. D. Kuang, C. J. Chen, D. Kirsch, L. B. Hu, Adv. Energy Mater. 2019, 9, 1901457.
- [2] X. Wu, S. Xia, Y. Huang, X. Hu, B. Yuan, S. Chen, Y. Yu, W. Liu, Adv. Funct. Mater. 2019, 29, 1903961.
- [3] C. Huang, P. S. Grant, J. Mater. Chem. A 2018, 6, 14689.
- [4] a) J. W. Wang, Q. Sun, X. J. Gao, C. H. Wang, W. H. Li, F. B. Holness, M. Zheng, R. Y. Li, A. D. Price, X. H. Sun, T. K. Sham, X. L. Sun, ACS Appl. Mater. Interfaces 2018, 10, 39794; b) L. Zhou, W. W. Ning, C. Wu, D. Zhang, W. F. Wei, J. M. Ma, C. C. Li, L. B. Chen, Adv. Mater. Technol. 2019, 4, 1800698.
- [5] a) R. V. Salvatierra, A. R. O. Raji, S. K. Lee, Y. S. Ji, L. Li, J. M. Tour, Adv. Energy Mater. 2016, 6, 1600918; b) L. B. Hu, F. La Mantia, H. Wu, X. Xie, J. McDonough, M. Pasta, Y. Cui, Adv. Energy Mater. 2011, 1, 1012; c) R. Elango, A. Demortiere, V. De Andrade, M. Morcrette, V. Seznec, Adv. Energy Mater. 2018, 8, 1703031; d) J. S. Wang, P. Liu, E. Sherman, M. Verbrugge, H. Tataria, J. Power Sources 2011, 196, 8714.



ADVANCED ENERGY

16146840, 2021, 22, Downloaded from https://advanced.onlinelibrary.wiley.com/doi/10.1002/nemm.202100601 by University Town Of Shenzhen, Wiley Online Library on [24/11/2025]. See the Terms

and Conditions

on Wiley Online Library for rules of use; OA

articles are governed by the applicable Creative Commons

www.advancedsciencenews.com www.advenergymat.de

- [6] a) B. Wang, J. Ryu, S. Choi, G. Song, D. Hong, C. Hwang, X. Chen, B. Wang, W. Li, H. K. Song, S. Park, R. S. Ruoff, ACS Nano 2018, 12, 1739; b) J. M. Kim, C. H. Park, Q. L. Wu, S. Y. Lee, Adv. Energy Mater. 2016, 6, 8; c) S. J. Cho, K. H. Choi, J. T. Yoo, J. H. Kim, Y. H. Lee, S. J. Chun, S. B. Park, D. H. Choi, Q. L. Wu, S. Y. Lee, S. Y. Lee, Adv. Funct. Mater. 2015, 25, 6029; d) Z. Wu, X. Han, J. Zheng, Y. Wei, R. Qiao, F. Shen, J. Dai, L. Hu, K. Xu, Y. Lin, W. Yang, F. Pan, Nano Lett. 2014, 14, 4700.
- [7] M. E. Sotomayor, C. de la Torre-Gamarra, W. Bucheli, J. M. Amarilla, A. Varez, B. Levenfeld, J. Y. Sanchez, J. Mater. Chem. A 2018, 6, 5952.
- [8] a) X. Wang, T. Y. Wang, J. Borovilas, X. D. He, S. Y. Du, Y. Yang, Nano Res. 2019, 12, 2002; b) Z. Zhao, M. Sun, W. Chen, Y. Liu, L. Zhang, N. Dongfang, Y. Ruan, J. Zhang, P. Wang, L. Dong, Y. Xia, H. Lu, Adv. Funct. Mater. 2019, 29, 1809196.
- [9] J. Hu, Y. Jiang, S. Cui, Y. Duan, T. Liu, H. Guo, L. Lin, Y. Lin, J. Zheng, K. Amine, F. Pan, Adv. Energy Mater. 2016, 6, 1600856.

- [10] L. Yang, K. Yang, J. Zheng, K. Xu, K. Amine, F. Pan, Chem. Soc. Rev. 2020, 49, 4667.
- [11] a) D. Q. Xue, R. Sethi, J. Nanopart. Res. 2012, 14, 14; b) J. Liu, D. G. D. Galpaya, L. J. Yan, M. H. Sun, Z. Lin, C. Yan, C. D. Liang, S. Q. Zhang, Energy Environ. Sci. 2017, 10, 750.
- [12] Z. X. Xu, J. Yang, T. Zhang, Y. N. Nuli, J. L. Wang, S. I. Hirano, *Joule* 2018, 2, 950.
- [13] S. N. S. Hapuarachchi, K. Wasalathilake, J. Y. Nerkar, E. A. Jaatinen, A. P. O'Mullane, C. Yan, ACS Sustainable Chem. Eng. 2020, 8, 9857.
- [14] a) J. Nam, E. Kim, K. K. Rajeev, Y. Kim, T.-H. Kim, Sci. Rep. 2020, 10, 14966; b) J. Ryu, S. Kim, J. Kim, S. Park, S. Lee, S. Yoo, J. Kim, N. S. Choi, J. H. Ryu, S. Park, Adv. Funct. Mater. 2020, 30, 1908433.
- [15] a) C. Hong, Q. Leng, J. Zhu, S. Zheng, H. He, Y. Li, R. Liu, J. Wan, Y. Yang, J. Mater. Chem. A 2020, 8, 8540; b) D. Kong, J. Hu, Z. Chen, K. Song, C. Li, M. Weng, M. Li, R. Wang, T. Liu, J. Liu, M. Zhang, Y. Xiao, F. Pan, 2019, 9, 1901756.